

## Biological Imaging Spectroscopy

Gregory Bearman, Jet Propulsion Laboratory, California Institute of Technology  
Richard Levenson, Cambridge Research and Instrumentation, Woburn, MA

### INTRODUCTION

Improved detectors, new electro-optical devices and vastly improved computational power for data analysis have fueled the recent interest in combining biology and spectroscopy. This review article will cover three aspects of biomedical spectroscopy. (1) Data acquisition: what instruments are available for acquiring an image cube and what are the performance trade-offs involved in choosing one over the other (2) Data analysis: what are some of the approaches for examining very large and multivariate data sets? We shall see that the remote sensing community, focused primarily on geology, has many tools that can be applied to biomedical data. (3) Applications: which current research areas in biology and medicine can exploit the power of imaging spectroscopy?

Light is composed of photons with different energies. While we can think of higher energy (shorter wavelength) photons as being “blue” and less energetic (longer wavelength) photons as being “red”, these color attributes are an artifact of the human visual system. In fact, there turns out to be no simple relationship between wavelength content of light and the color we actually perceive. This is (in part) because our eyes (and conventional color film and color digital cameras) allocate visible light, no matter how spectrally complex, into only about 3 different color bins: red, green and blue (RGB). Light with completely different spectral content can have precisely the same RGB coordinates, a phenomenon known as metamerism. For example, red light and green light can combine to form yellow. If we see a yellow object, we cannot tell if the color is spectrally pure (as it would be if it were created by a prism or rainbow) or if it arose from a mixture of red and green...

Researchers have used human color vision to interpret images since the first microscope. Although we perceive three spectral bands and cover a relatively narrow range, the human eye is quite sensitive to subtle color differences within that range. When exogenous dyes were used to differentially color cellular structures or molecules, the interpretation still relied on color vision, and more recently, on electronic color cameras. The addition of fluorescent dyes to the microscopist’s tool kit began to push the limit of color vision, electronic or otherwise. The standard detection toolkit of fluorescence microscopy is an array of dichroics, filter cubes and other filters designed to separate multiple colored probes, either in absorption or fluorescence emission. Increasing the number of probes, as biologists want to do, creates so much spectral overlap that filtering cannot separate the probes; i.e., color images of fluorescent probes that differ only slightly spectrally appear the same. In that case, we need to use some sort of spectroscopy.

Spectroscopy usually uses single point detectors that cannot easily sample large areas or small areas at high resolution. On the other hand, imaging spectroscopy can spectrally image large areas, combining the function of a camera (recording spatial information) with that of a spectrometer. These devices can measure the spectral content of light at every point in the image: a 1,000 by 1,000 pixel sensor provides

one million individual spectra. Once a spectral stack is acquired, mathematical approaches ranging from simple to very sophisticated can be used for analysis. Analysis of fluorescent microscopy uses spectral signatures to match each pixel with one of the known probes used in the experiment. Imaging spectroscopy tells us *what* is *where*.

Once properly calibrated, these images can be used to obtain corrected spectrum for each image pixel, which can then be used to identify components in the target. For the geologist, imaging spectroscopy yields compositional maps of geologic sites, showing *which* minerals are *where*<sup>1</sup> or to determine the composition of the rain forest canopy<sup>2</sup>. It can detect agricultural pests<sup>3</sup> or drought stress, or fertilizer application levels. Spectral imaging has uses in industrial process control, in detection of ordinarily invisible bruising in fruit, in assessing the viability of transplanted organs<sup>4-5</sup> in uncovering forgeries, and so on. Finally, modifications in existing designs and novel approaches have made spectral imaging easy to accomplish with a microscope; this combination has promising applications in surgical pathology and molecular biology. Fluorescent dyes have recently become available which will increase the usefulness of spectral imaging in a variety of areas, including high-throughput screening, genomics, and clinical diagnostics.

### ***Spectral Image Cubes***

Simply put, an imaging spectrometer acquires the spectrum of each pixel in a 2D spatial scene. As shown in Figure 1, the easiest way to think of such a scheme is band sequential imaging, in which multiple images of the same scene at different wavelengths are acquired. A key point is that the spectra be sampled densely enough to reassemble a spectrum [commensurate with the needs for analysis]. A remote sensing instrument may take hundreds of more images over the visible to near-infrared (NIR) range. There are many technological means of obtaining this data and this article will present a catalog of current technologies. The images are typically stacked in a computer, from the lowest wavelength to the highest, to create an image cube of the dataset. The spectrum of a selected pixel is obtained by skewering it in its third dimension, wavelength, as the inset in Figure 1 shows. While there are many ways of acquiring and storing the data, this representation is band-sequential (often termed BSQ), in which the images are stacked like a deck of cards and resembles a cube with sides  $x$ ,  $y$  and  $\lambda$  (wavelength). Even if the data is acquired in some other fashion, it can be reconfigured into this mode. Two other data modes are band-interleaved-pixel (BIP) and band-interleaved-line (BIL). In BIP, the spectra of successive pixels are stored sequentially. This is advantageous for computation, as the spectrum of each pixel can be read directly, as opposed to band-sequential data where one has to read in the entire cube to calculate a spectrum of any given pixel.

## INSTRUMENTS

Before describing specific instruments, it is worthwhile to compare spectral imaging with what can be accomplished using standard imaging systems based on conventional RGB sensors. Because most such systems rely on single chip cameras, color images can be acquired in a single exposure, typically at near-video rate. In contrast, most spectral systems require a series of exposures, so improvements in

the quality or utility of the data collected should be large enough to justify the potential penalties in cost and throughput and data acquisition time.

For example, while earlier systems for automated or assisted immunohistochemistry quantitation, a relatively simple problem in color analysis, used grayscale cameras and two or more color filters somewhere in the light path, recent approaches exploit RGB cameras and analytical strategies of varying levels of sophistication and complexity. With automatic thresholding operations, Ruifrok<sup>6</sup> was able to differentiate between a DAB (brown) stain alone, DAB plus hematoxylin (blue) and hematoxylin alone. More recently, this group has shown that conversion of RGB images into optical density units allowed for more accurate discrimination. However, RGB sensors have intrinsically broad and overlapping regions of spectral sensitivity for their three color channels, and this adversely affects unmixing accuracy, especially when separation of similar chromogens is being attempted. Thus, for example, a dense brown stain can generate a signal in the post-analysis red channel<sup>7</sup>. While it may be possible to unmix red, brown and blue using only 3 input images, the optimal wavelengths and bandwidths will differ from the broad channels provided by standard RGB imaging systems.

There are additional technical and practical problems with conventional color imaging. First, many color cameras use a CCD that produces a color-encoded analog signal that is digitized by a computer video board into R, G and B pixel intensities. The fidelity and consistency of such a system can be variable. Section-to-section variability, along with interactions with camera controls such as automatic gain control, can induce fluctuations in the image quality. Because the color of a stained object is a product of the stain's transmittance and the camera's spectral response, it is possible that dyes differing in spectral properties could be sensed similarly by the camera and thus be indistinguishable. Finally, the spatial resolution of single-chip color CCD cameras is typically lower than that of monochrome cameras with the same pixel count because of the color mask and interpolation routines that merge information from 3 or more pixels when determining RGB and intensity values

True imaging spectrometers, in some fashion, acquire a three-dimensional data set, spatial (2D) and wavelength as third dimension. The approaches for instruments traditionally involved scanning one of the dimensions, either acquiring a complete spectrum for each pixel (or line of pixels) at a single shot and then spatially scanning through the scene, or alternatively, taking in the complete scene in a single exposure, and then stepping through wavelengths to complete the data cube. While typically the light emerging from the imaged object is filtered for spectral content, it is also possible to control the spectral content of the illumination. Recently, other instruments have been developed that acquire both spectral and spatial information in a single exposure, although with some trade-offs.

Figure 2 shows an image cube and how different cuts through the data illustrate the different approaches. Some of the terminology comes from the origins of imaging spectroscopy, which involved performing remote sensing from a moving platform. For example, the whiskbroom imaging spectrometer is one in which a single point is scanned perpendicular (cross-track) to the direction of motion. The spectrum of each pixel is acquired with a spectrometer and the data is taken a spectrum at a time pixel-by-pixel along a line. The name comes from the fact that the path of the scanned pixels resembles that of a whiskbroom in action. Similarly, a pushbroom spectrometer images a slit onto a focal plane array; the spatial dimension occupies one axis of the array and the spectrum for each pixel is

spread out perpendicularly to it. A complete image is acquired one line at a time as the slit is scanned in the direction of motion. In biological imaging, point-scanning and slit-scanning confocal microscopes use similar image collection geometries respectively. In addition to these techniques, which collect spectral data directly, there are other modalities that require mathematical processing of the intermediate data.

We will break up the discussion of instrument types into four general types:

1. **Spectral scanning:** These use electro-optical devices such as liquid crystal or acousto-optic tunable filters, as well as filter wheels and project complete images onto CCDs or other focal plane arrays. Spectral scanning can also be achieved by controlling the spectral content of the illumination source rather than filtering the remitted light.
2. **Spatial scanning:** These use either pushbroom or whiskbroom configurations with prisms, gratings or beam-splitters to create spectral discrimination.
3. **Interferometric:** These typically (but not always) acquire a 2D image and scan optical path differences in some manner to obtain a complete interferogram at each pixel; the data needs to be mathematically converted into spectra in wavelength space.
4. **Miscellaneous:** These include instruments such as the computed tomographic imaging spectrometer and a polarization-dependent rotogram device

**1. Spectral Scanning Instruments.** Such instruments are easy to understand and have very simple optics. They consist of imaging optics, a tunable filter of some sort for spectral selection (or a tunable light source) and a camera. Since the components can be in-line or folded, such systems can be made rather compact, suitable for mounting on microscopes or other instruments. The tunable filter can be a mechanical filter wheel, a linear variable filter or an electro-optical filter that can be tuned electronically.

**Fixed Filters:** The simplest implementation of an imaging spectrometer incorporates a filter wheel equipped with a set of fixed bandpass filters in a rotating mount. A variant often necessary for fluorescence imaging would substitute a set of filter cubes (combinations of dichroic mirrors, excitation and emission barrier filters) for a simple filter wheel. For applications where there are a relatively small number of wavelengths needed, pre-set and invariant, this can be a useful technique. For example, Speicher et al.<sup>8</sup> has demonstrated fluorescence-based spectral imaging with a filter system generating a combinatorial library of 27 colors, enough to paint all the human chromosomes. Furthermore, compared to other approaches, a filter wheel can be relative inexpensive and is also quite light efficient (although the latter consideration is not straightforward and can depend on the degree of spectral cross-talk between channels tolerated). These instruments have limitations. (1) They lack spectral flexibility, since only a relatively small number of wavelength choices are available in any one configuration. While one could make the filter holder larger to accommodate more filters, this increases the size and expense commensurately. (2) The performance of the filters can change unpredictably over time due to aging. (3) Switching speeds can be low. (4) Moving parts create noise and vibration. (5) There can be image registration problems due to misalignment of filters.

**Linear Variable Filters:** A linear variable filter can also act as a spectral filtering element for an imaging spectrometer. For such filters, the transmission varies linearly along the filter; at any wavelength,  $\lambda_0$ , (or position along the filter), the local transmission is a bandpass filter with a width that is a fixed fraction of  $\lambda_0$ . That width is 1-1.5%, depending on the filter, so a typical bandwidth is ~4-10 nm over the visible spectrum. One vendor, OCLI, has marketed a spectrometer without a grating, using a linear filter directly on top of a linear CCD detector array. There are similar versions known as circular variable filters (CVF) in which the transmission changes with rotational angle of the filter.

An optical system with a beam waist can use a linear or circular variable filter to create an imaging spectrometer by inserting the filter at the location of the minimum spot size. Since the filter's transmission is spatially dependent, a large spot size would give a large and spatially varying bandwidth, so the filter is located at a beam waist to reduce the resultant spectral smearing. In this mode, the filter acts like a filter wheel with a large number of filters. Images are acquired at each wavelength and filter translated or rotated to the next wavelength. Kairos Scientific [www.kairos-scientific.com] has developed a system using a circular variable filter that mounts onto a microscope. Surface Optics Corp. (San Diego, CA) has developed an innovative variant based on TDI (Time Domain Integration) that reads out an imaging array row-by-row synchronized to the motion of a spinning CVF (to avoid the problem of spectral smearing). In conjunction with algorithms implemented in hardware, their instrument is capable of acquiring *and processing* 30 image cubes per second.

**Tunable Filters:** As the name implies, these devices can tune their spectral passband electronically, and without moving parts. Advantages include quiet and vibration-free operation, switching speed, spectral selectivity, spectral purity and flexibility. There are several important criteria that such filters need to meet. (1) Since the entire image is being filtered, the filter wavelength needs to be constant over the entire image or meet some lower limit for edge effects. (2) Introduction of the filter into the optical path cannot introduce (significant) image distortion. (3) The tuning time has to be commensurate with the dynamics of the experiment. (4) Out-of-band rejection must be sufficiently good that dim in-band signals are not contaminated by out-of-band intrusions<sup>9</sup>.

**a) Liquid crystal tunable filters (LCTFs):** LCTFs use electrically controlled liquid crystal elements that transmit a certain wavelength band while being relatively opaque to others. The rejection of the unselected wavelengths, without further manipulation, is about  $10^4:1^{10}$ . The band pass can be as narrow as 1 nm or even less, and the spectral range with a single device can range from 400 nm to 720 in the visible

Mode of action: The LCTF is based on a Lyot filter, a device constructed of a number of static optical stages each consisting of a birefringence retarder (quartz for LCTFs) sandwiched between two parallel polarizers. A stack of stages function together to pass a single narrow wavelength band... As the incident linearly polarized light traverses the retarder, it is divided into two rays, the ordinary and extraordinary, that has different optical paths, given by

$$\Gamma(\lambda)=2\pi*\Delta d/\lambda$$

where  $\Delta$  is the birefringence and  $d$  is the thickness. After transmission through the retarder, only those wavelengths of light in phase are transmitted by the polarizer and passed onto the next filter stage. The transmission of a stage is

$$T(\lambda) = \cos^2[\Gamma(\lambda)/2]$$

as illustrated in Figure 3. The overlap of these continuously varying transmission curves determines which wavelengths are passed by the filter stack as a whole. To introduce tunability, a liquid crystal layer is added to each stage, as in Figure 3a, which by creating minor changes in retardance affects the position along the spectrum where the curves constructively interact. Tunability is provided by the partial alignment of the liquid crystals along an applied electric field between the polarizers; the stronger the field, the more the alignment and the greater the increase in retardance. Tuning times for randomly accessing wavelengths depend on the liquid crystal material used and the number of stages in the filter. At the moment, commercial devices use nematic components that result in tuning times of approximately 50 to 75 ms.

Polarizers introduce some restrictions into the operating range of an LCTF filter. Plastic sheet polarizers function below  $\sim 730$  nm and Polarcor glass polarizers are usable from  $\sim 630$ -1700 nm. In practical terms, the VIS to NIR range can be covered from 420 to 1800 nm using 3 devices available from CRI, Inc. that address the following spectral regions: 400-720 nm, 650-1100 nm and 850-1800 nm, each device covering about 1 octave (2-fold spectral range).

While the position of the bandpass is actively tunable, its width is fixed and depends on the construction of the device. A typical bandpass in the visible is  $\sim 10$  nm, which is wavelength-dependent ( $\propto \lambda^2$ ; 10 nm @ 550 nm grows to 16 nm at 700 nm). Since the bandpass is related to the number of stages in the device, any bandpass can be designed and fabricated, from  $16 \text{ cm}^{-1}$  to 50 nm. The  $16 \text{ cm}^{-1}$  device has been used for Raman imaging spectroscopy<sup>11</sup>. The devices are rather spectrally flat over a relatively large aperture (38 mm). Like the AOTF, the LCTF is polarization-sensitive, which reduces the transmission by half, unless optical means are provided to harvest both polarization states.

LCTFs work best in a collimated or telecentric optical space, as the maximum f-number that provides an off-axis shift of less than 2 nm at the filter edge is  $\sim 2.5$ . Since the device operation depends on interference effects, photons that are significantly off-axis have a different optical path than on-axis photons, creating edge effects. However, since many optics are inherently slower than  $f/2.5$ , they can be used before optical elements. One of the authors (Bearman) has taken a number of image cubes of remote scenes with an LCTF mounted in front of a Nikon 135-mm lens operated at  $f/4$ , as have others. Similar arrangements are also available commercially from Opto-Knowledge Systems, Inc ([www.oksi.com](http://www.oksi.com)).

The LCTF approach has been used to create image cubes for biological imaging (see below), confocal microscopy<sup>12</sup>, agriculture and imaging archeological documents such as the Dead Sea Scrolls<sup>13</sup>.

#### **b) Acousto-optic tunable filter (AOTF):**

An acousto-optic tunable filter (AOTF) uses the interaction between a crystal lattice and an acoustic wave to diffract an incoming beam into a fixed wavelength. As an applied acoustic wave propagates through the crystal, it creates a grating by alternately compressing and relaxing the lattice. Those density changes create a local index of refraction changes that acts like a transmission diffraction grating, except that it diffracts one wavelength at a time, so it behaves as a tunable filter. In practice, the undiffracted zero-order beam is stopped with a beam stop and the monochromatic diffracted beam is available. The wavelength of the diffracted beam is changed by changing the frequency (and wavelength) of the acoustic wave, thereby also adjusting the grating spacing. In addition, if multiple RF frequencies are launched into the crystal, then combinations of frequencies can be diffracted simultaneously; in this it is more flexible than LCTFs, which generate only a single bandpass at a time.

For visible wavelengths in a tellurium oxide crystal, the applied acoustic wave is RF and can be switched very quickly (typically in less than 50  $\mu$ s) compared to other technologies. Unlike an LCTF in which the bandwidth is fixed by the design and construction, an AOTF can vary the bandwidth by using closely spaced RFs simultaneously. There are several standard problems with AOTFs, some of which have been successfully addressed: blurred images and poor out-of-band rejection ( $<10^{-3}$ ). The acoustic wave spreads as it propagates through the crystal so diffracted rays leave at a variety of angles, resulting in blurred images. Use of a compensating prism<sup>14</sup> has significantly improved resolution. Narrowing the acceptance angle and attending to details of crystal fabrication can also overcome image blur and shift, albeit at a cost in light throughput<sup>15</sup>.

Both the AOTF and LCTF imaging spectrometers share an important attribute: they make it easy to get very good signal-to-noise spectra. This is due to the band-sequential nature of their operation. When spanning a wavelength range, say 400-720 nm, the sample may have a considerable variation in reflectivity or transmission over that range. In addition, at the blue end of the spectrum CCD sensitivity declines, as does the illumination intensity of many laboratory light sources. As a result, there is typically less signal in the blue relative to the red or green part of the spectrum. However, that can be compensated for by longer integration times at the wavelengths with reduced signal, something not possible with many other devices. In fact, the ideal way to operate a BSQ imaging spectrometer is to set a pixel data target value and integrate at each wavelength as long as necessary to obtain that value, maintaining the SNR at each wavelength. In that case, the *model* raw data spectrum of the target pixel would be a straight line, with the real data contained in the varying integration times for each wavelength. This is a major advantage, especially when there are no restrictions on the data acquisition time.

Spectral leakage can contaminate the acquired spectra. One advantage of the LCTF is a high rejection ratio for out-of-band transmission ( $10^{-3}$ - $10^{-5}$ ), critical for recovering spectra that can be compared with those from other laboratories or with standard spectral libraries. LCTFs can be fabricated with larger apertures than AOTFs, although that is not an issue for integration into microscopes, which do not need the large aperture. One the other hand, their major drawback is longer tuning time relative to an AOTF:  $\sim$ 30-50 ms vs. microseconds for the AOTF. There is a switching mode for LCTFs that is somewhat faster, around 20 ms, but that is for a limited palette of perhaps 3-4 wavelengths. For situations in which the integration time is photon-limited and the exposure time is  $\geq$ 50 ms, the tuning

time of either device becomes less of a bottleneck for data acquisition. In fact, it is usually the camera data transfer rate that dominates acquisition time when light is ample.

### **Pushbroom**

Lightform, Inc.<sup>16</sup> has developed a pushbroom imaging spectrometer that is designed to mount to a C-mount camera port. It collects a slit image from the object onto a 2D camera in which the spatial information is displayed along one axis and wavelength information along the other. Wavelength dispersion is provided by a prism. This approach is well suited for scanning gels or searching an object for specific spectral features since the entire spectrum of each pixel in the slit image is available in real-time. Since gels are too large to image easily, they can be mechanically scanned with this system. With this approach, the user does not have to collect an entire image cube, but can assemble an image that records hits only for the spectra of interest. If there is a known spectral feature, that feature can be identified in each spectral line scan in real-time and used to assemble a classified image without having to acquire the entire spectral cube for the whole image field.

### **Interferometers**

Rather than scanning in wavelength space, one can also scan in optical-path-difference space and capture an interferogram for each pixel, which is then inverted via the FFT algorithm to obtain an image cube in wavelength space. Several devices have been developed and one is available commercially. Although seemingly different from instruments that acquire sequential wavelength images, many of the interferometric devices are similar in spirit and suffer from similar problems. Like the BSQ imagers, interferometric imaging spectrometers also require acquisition of many images, and sometimes an order of magnitude more images. For so many images, the data acquisition time may become limited by camera image transfer time.

Applied Spectral Imaging of Israel was perhaps the first company to make a commercially available imaging spectrometer. The device is a common-path Sagnac interferometer in which the interferogram is spread out over a 2-dimensional sensor<sup>17</sup>. An optical element changes the optical path difference (OPD) in stepwise fashion, while a CCD (or other technology) focal plane array captures the resulting interference pattern at each step. Since the interferogram moves with each OPD image, object motion is a challenge for this instrument. If the object moves and the images are corrected by re-registering the spatial content to compensate, any errors will show up as incorrect interferograms and propagate into the spectra after inversion. The ASI instrument has been used for cytogenetics<sup>18</sup> and cell pathology<sup>19</sup>, to name a few applications.

Another interferometric device has been developed by Itoh<sup>20</sup>. This device uses a tilted and wedged lens array and mirrors to acquire all the necessary images at different OPD *simultaneously* on a 2D imager. Itoh has demonstrated imaging of rapidly moving objects with this approach, a laser ablation plume and rotating (1800 RPM) targets. Since all the multiple images have to be acquired on a single detector, there is a trade-off between image size and spectral resolution.

One problem with interferometers is that of the center burst ( $OPD=0$ ), which is quite bright relative to the rest of the fringes. Since the detector is an imager, the integration time or illumination intensity has to be reduced sufficiently to avoid saturation (or blooming) for pixels at the center burst, thereby reducing the fringe contrast further out in the interferogram. The reduced fringe contrast decreases the signal and resulting in increased noise in the image cube in wavelength space.

There has been considerable discussion in the literature about the relative photon efficiency of interferometers compared to scanning instruments. Although on the surface the interferometer appears to have a substantial advantage over other approaches due to the fact that it collects all the spectral information simultaneously<sup>21</sup>, several papers<sup>22, 23</sup> have argued that for real instruments with read-noise and other noise sources, this advantage disappears in most imaging regimes. Furthermore, in the spectrally sparse scenes typical of fluorescence imaging, in which signals occupy only a fraction of the total spectral range, the ability of tunable filters to capture images only at informative wavelengths improves their performance relative to interferometer-based approaches that have to collect all wavelengths, informative or not.

## **Other Approaches**

### **Rotogram**

Microcosm Inc. (Columbia, MD) recently developed an imaging spectrometer using a new spectral imaging technique based on the phenomenon of the dispersion of optical rotation<sup>24</sup>. Figure 4 schematically represents the optical layout of the HSI with polarizers at the input and output of an optically active rotating medium... The polarization plane of linearly polarized light is rotated during propagation through the optically active rotator element so that the rotation angle,  $\phi(\lambda)$ , of the plane of polarization of the output light depends on the wavelength of the light and the path length through the optically active rotator element. The path length through the active medium can be varied, thus incrementally increasing the rotation of each wavelength component present. After passing through the output polarization analyzer, an intensity function is measured for each incremental polarization path length. This arrangement permits the wavelength-dependent polarization rotation to be uniform over a large two-dimensional aperture so a CCD is a suitable detector. The intensity function resulting from a stack of images can be analyzed at any pixel in the image by mathematical methods to yield a highly accurate spectrum at each point in the image. Like several data acquisition methods, there is some computation required for reconstructing the image cube.

Like the LCTF or the AOTF, the transmission is polarization-dependent. The unit will transmit 40-45% of the incoming unpolarized light depending upon the rotator material. If the incoming light is polarized, then the throughput efficiency can reach 85-90%. The HSI can have a large clear aperture that provides excellent light coupling through the device for the use of wide-field spectral imaging. It does not induce any beam deflection or image movement and can be used in-line with almost any imaging system. In a different configuration, the HSI is suitable for use with a point-scanning device such as laser scanning microscopes or alternatively the classical push-broom and whisk-broom configurations are easily achieved and offer high speed and arbitrarily high spectral resolution depending on the design and application.

### **Computed Tomographic Imaging Spectrometer (CTIS)**

A recent approach to imaging spectroscopy is tomographic imaging, as illustrated in Figure 5. With this technique, diffractive optics disperse the spectral and spatial information of each pixel onto an imaging sensor; an image cube in wavelength space is reconstructed from a *single* image. Since it turns out that the mathematics of the reconstruction is the same as tomographic imaging, such devices are known as computed tomographic imaging spectrometers (CTIS). Originally proposed by several researchers<sup>25,26</sup> in the early nineties, they have been further developed by Descour et al.<sup>27</sup>.

A diffractive optical element operating at multiple orders creates an array of images on the sensor. Development of techniques for fabricating the grating with e-beam lithography has been the main driver in development of this instrument<sup>28</sup>. It is important to note that each image is not simply composed of single wavelengths; that information is multiplexed over the entire array. Figure 5 shows how the spectrum of a single pixel is distributed by the diffractive disperser. Note that there is a zero-order image which can be used for focusing, a difficult task for many spectral imagers. A calibration matrix is necessary to perform the reconstruction; it is obtained by measuring the location on the image plane of pixels in the object plane at different wavelength with a movable fiber optic coupled to a monochromator. A CTIS can operate over a large wavelength range, easily from 400-800 nm and with the proper detector can operate in the IR or UV. The data from a single image can be reconstructed in a variety of ways to adjust image size and wavelength bands. For example, an image can be reconstructed with 128 x 128 pixels with 20 bands or 64 x 64 pixels and 32 bands, using the *same* dataset. The only difference between the two reconstructions is the calibration matrix.

A major advantage of the CTIS is speed. Since it takes a single image that contains all the spectral/spatial data, it can be run at video rates<sup>27</sup>, assuming sufficient light and a high-speed camera (since a large pixel array is typically required by this method). This potential speed makes it suitable for studies such as endoscopy and rapid processes that other instruments cannot handle. Alternatively, it is useful for collecting radiometric data, since all wavelengths are acquired simultaneously. A major issue with spectral imagers has always been bandwidth--they tend to produce enormous amounts of data that present downlink or transmission problems. For example, a satellite hyperspectral imager can produce hundreds of gigabytes of data a day. In the same vein, a remotely sited or operated imaging spectrometer can easily present significant bandwidth demands for data transmission in a power limited environment [power=bandwidth for telecommunications].

CTIS devices have been used for some real-world imaging studies; Descour et al. have demonstrated radiometric pH-imaging with standard probes using a CTIS<sup>29</sup> while de la Iglesia et al.<sup>30</sup> used one for toxicology studies. In both cases, the device allowed capture of the entire spectrum of fluorescent probes at once.

### **Hadamard Transform Imaging Spectroscopy**

Hadamard transforms have been used for spectroscopy for some time<sup>31</sup> and have been adapted to fluorescence microscopy. The fabrication of large-format liquid crystal spatial modulators has made

this application possible as they can to create the Hadamard masks rapidly and with no moving parts. In a series of papers, Jovin and colleagues have developed this implementation of imaging spectroscopy and microscopy<sup>32</sup>.

Like the CTIS or an interferometer, the Hadamard transform spectrometer requires computation to reconstruct the image cube in wavelength space. However, it also requires a large number of images, for example, Hanley reports acquiring 511 images in ~11 minutes and 5 minutes of computation to transform the data. Clearly some of the data time can be reduced by increasing optical efficiency, but like the interferometer, the basic nature of the device requires many images.

### **Spectral Source**

For microscopy brightfield applications, it is possible to accomplish spectral imaging by tuning the illumination light as well as filtering or otherwise analyzing the remitted light. Monochromators (usually relying on diffraction gratings and white light sources) are available for such purposes. However, as the name implies, monochromators provide illumination consisting only of one spectral band of light at a time. However, it is possible to create sources that are more flexible and can produce illumination of any desired pure wavelength (like a monochromator) or any selected mixture of pure wavelengths simultaneously, with white light output an easy option<sup>33</sup>. The resulting images can be collected by a high-resolution gray-scale CCD camera and interpreted using appropriate algorithms and displays. It can be used to create a complete spectral image cube for a sample by taking sequential images while illuminating with a series of pure wavelengths, with greater ease and economy than by means of devices on the imaging path, such as tunable filters or interferometers. An advantage over tunable filters in some applications is that contamination of individual bands by out-of-band light is minimal. Furthermore, using software approaches such as projection pursuit vectors, or principal components to define specific illuminants, the sample can be illuminated with a precisely controlled mixture of wavelengths so that the image presented to the detector is a linear superposition of the sample properties at many wavelengths. Thus, spectral discrimination that would previously have required the collection of complete spectral cubes might require acquisition of as few as 1 to 3 matched spectral images per field. Data acquisition is simplified, and, since spectral processing is being performed optically rather than computationally, both acquisition and analysis times are greatly reduced...

### **Multispectral confocal microscopy**

Much biology today uses confocal microscopy as a major tool to provide high-resolution 3D imaging of cells and tissue. Considerable effort has gone into developing optics and software to provide diffraction-limited imaging in commercial instruments. Similar effort has been expended on fluorescent probes to illuminate cellular activity. Can we apply imaging spectroscopy to confocal microscopy? The answer is yes, but with some limitations.

Laser scanning confocal microscopes (LSCM) raster a laser spot across the object, obtaining a full image a point at a time, similar to the way a whiskbroom imaging spectrometer operates. Since a pinhole, present in the optical path to provide confocality, attenuates the signal considerably, a PMT

is typically used as a detector to provide sufficient gain and reasonably short dwell-time per pixel. To obtain an emission image cube of a fluorescently labeled sample, there are two options. Since the image is already being scanned, if we can somehow filter emission wavelength prior to detection we can assemble an image cube. This was done recently by inserting an LCTF in front of the PMT in a LCSM and stepping through the emission wavelength range<sup>12</sup>. One could also use an AOTF as the filtering element. While serviceable, this is not a practical method, as it requires multiple scans at different wavelengths to acquire a full image cube. Aside from the significantly increased time for assembling a z-stack, the repeated scans can cause excessive photobleaching.

For an LCSM, the best data collection scheme would be to acquire the entire spectrum from each spatial pixel as it is scanned, making it in effect a whiskbroom imaging spectrometer. In this approach, the instrument collects an entire image cube in the same time as a single spatial scan. Zeiss has recently introduced a spectral imager that obtains the spectrum for each pixel as the LCSM scans through the image. Due to scanning nature of the data collection and the need for gain, it would be largely unrewarding to adapt other spectroscopic techniques to an LCSM.

However, one could image adapting an interferometric or tunable filter device to a confocal microscope that uses a Nipkow disk since these present an entire image to a CCD. Thus, any spectroscopic device that can be interposed before a CCD camera should be compatible with this or similar confocal designs. However, any method that requires a lot of images may pose practical problems when doing real experiments due to the possibility of photobleaching and the time involved in acquiring an  $(x,y,z,\lambda,t)$  image stack.

## Data Analysis

### Image Analysis.

A number of freestanding spectral analysis tools are available commercially or as free-ware. These include Research System International's ENVI™, and MultiSpec™<sup>34</sup>. Other programs can be assembled by the sophisticated user with resources available in such packages as MatLab™ such as the statistics, chemometrics and image analysis toolboxes, supplemented with researcher-generated MatLab-compatible algorithms downloadable from various internet sites. Still others are available bundled with commercially available spectral imaging hardware (OKSI, Kairos Scientific, Spectral Dimensions, ChemIcon, etc.). These software tools will not be described further, except for some aspects to be touched upon in the following discussion.

One of the appeals to developing spectral imaging systems or applications is the richness of the datasets, comprising both spatial and spectral information, which invites the use of intriguing analytical tools. Indeed, many of the algorithms, such as automatic clustering tools, being developed for use with genomics datasets (such as the huge expression arrays) are applicable to spectral cubes, with the proviso that these methods do not encompass any of the spatial content to be found in the images. Methods attempting to link spatial and spectral data are under development<sup>35</sup>. Another thread in current investigations is determining how to select the minimum number of wavelengths needed to accomplish specific tasks<sup>36</sup>. While it may seem intuitive that more spectral data and higher spectral

resolution may provide increased analytical precision, this is often not the case. Many wavelengths may be “uninformative,” and their inclusion in the dataset merely adds noise. This consideration is partially related to the so-called “curse of dimensionality,” which also deals with consequences of the huge internal volumes of the hyperspheres that can be used to represent high-dimensional datasets<sup>37</sup>. (This is more of a problem in remote sensing, in which data sets can contain images at hundreds of wavelengths.)

For the relatively simple problems posed by imaging in the visible range, and where the targets may be simply defined fluorescent dyes or chromogens, one may be able to lower the number of wavelengths acquired to approximate the number of distinct species sought in the image. Thus analytical techniques can be used not only to work with the datasets but also to shape how they are collected. At the limit, spectral flexibility can be used simply to provide a capability to select one or more specific wavelengths for the purposes of increasing contrast or enhancing the utility of straightforward image-analysis tools. In a recent publication, Ornberg et al.<sup>38</sup> describe using a tunable filter to identify optimal wavelengths for separating signal from background in samples stained with a single chromogen plus background stain. Using a simple processing routine, the authors were able to collect and analyze 2-3 images per minute.

### *Analysis of Spectral Images*

Assuming that more than a couple of wavelengths have been collected, the task of analysis usually involves classification, unmixing, or both. Classification involves the assigning of each pixel to one or more spectrally defined classes (or to an “unclassified” class, *pace* Bertrand Russell). Classification is equivalent to spectral segmentation; it is an *exclusive* operation in which a pixel or object is assigned to a *single* class using one or more of a variety of metrics. On the other hand, when pixels can be or are composed of more than one spectral class, as is often encountered when multiplexed protein or nucleic acid probes are used, then the pixels have to be “unmixed,” yielding estimates of the proportion of each class present. Overall, the steps involved typically consist of:

- 1) Detection and/or selection of appropriate spectra for subsequent analysis;
- 2) Spectral classification or pixel-unmixing.

Pixel Classification. There are several approaches to classifying pixels in a spectral image. The minimum squared error method compares the spectra at each pixel in the image with a set of reference spectra, choosing the most “similar” using a least-squares (Euclidean distance) criterion. This metric compares spectral means; other distance-metrics such as Mahalanobis distance<sup>39</sup> can be used that are sensitive to higher order statistics such as class variances. Related approaches convert spectra into  $n$ -dimensional vectors, and the angles between such vectors can be used as measures of similarity<sup>40</sup>. Determining which spectra to use for the classification procedure is not always straightforward. In simple cases, the reference spectra can be selected from obvious structures in the image (foci of cancer vs. normal cells, for example) or from established spectral libraries. Alternatively, informative spectra can be extracted using statistical analysis methods, such as principal component analysis (PCA) or clustering methods<sup>41</sup>. Instead of using a classified pseudo-color display, spectral similarity can also be

illustrated by mapping the degree of similarity using gray-scale intensity. This operation can reveal otherwise unapparent morphological details<sup>42</sup>.

**Pixel-Unmixing:** Spectral classification methods are suitable for images in which no pure spectral components are likely to exist, such as in histologically stained samples. In other types of images, such as those generated by immunofluorescence or in-situ hybridization procedures, multiple distinct spectral signals may co-exist in a single pixel to form the detected signal. Spectrally mixed pixels result when objects cannot be resolved either at an object boundary (spatial mixture), when more than one object is located along the optical path (depth mixture), or when multiple probes are co-localized within a pixel. In fluorescence, due to the additive nature of the light signal, the observed spectrum is a linear mixture of the component spectra, weighted by the amount of each probe. A linear combinations algorithm can be used to unmix the summed signal arising from the pure spectral components, to recover the weighting coefficients. Given an appropriate set of standards, the algorithm can quantitate the absolute amount of each label present<sup>43</sup>.

In contrast to fluorescence images, imaging multiplexed samples (such as immunohistochemistry studies) in brightfield must take into account the behavior of absorbing chromophores that, rather than being additive, subtract signal from the transmitted light in a non-linear fashion. Conversion of the brightfield image from transmittance to optical density (OD), a straightforward mathematical procedure, permits the use of the same linear unmixing algorithms that work with fluorescence.

*Automated end-member detection:* How does one select which spectra to use for unmixing? In many cases, this is easy. If one is doing standard immunofluorescence studies, the spectra of the fluorophores, imaged one at a time, can be stored in a spectral library and used to unmix images in which multiple fluors are present. But what if one does not have pure spectral species to work with, for example, if a single, multiply labeled image is available, or if, to change applications, one is trying to analyze a remote scene about which there is little *a priori* knowledge available? There are tools that can identify the pure spectral species present in an image, without *a priori* knowledge, by deconstructing the spectral content into its presumed components. ENVI™ provides a tool based on convex hull analysis that considers spectral endmembers (the pure species) to occupy the periphery of a data cloud all of whose mixed species must fall within, rather than on the surface. The cloud (in which each pixel's location is determined by its spectral content in *n*-dimensional space) is rotated randomly and projected onto a hyperplane. Pixels that repeatedly end up on the periphery after multiple projections are considered to be endmembers and can be used to unmix the image. This procedure can be quite time-consuming. Another specialized utility, N-FINDR<sup>44</sup> uses an analytical approach rather than multiple projections, and accomplishes the same task quite efficiently.

*Dimensionality reduction and automated cluster analysis:* Spectral data, as noted above, can be expressed as points in hyperspace. Spectrally similar pixels will cluster together and algorithms, some of which are similar to those used for analyzing genetic expression arrays, can be used to identify such clusters, which might represent meaningful bases for spectral classification<sup>45,46</sup>. Frequently, such analysis is either impossible or inefficient when all wavelengths are included in the dataset. Because there is a great deal of covariance in typical datasets (i.e., the intensity at one wavelength predicts to a high degree the intensity at neighboring wavelengths), the number of dimensions needed to express the

actual information content in a dataset is often far less than the number of dimensions in the dataset itself. Principal component analysis (PCA) is one of a family of statistical tools that can identify the most informative combinations of wavelengths (by rotating the basis vectors of the original dataset), and can segregate signal from noise (with some major limitations). Typically, the dimensionality of a 25-wavelength image cube of a standard histology sample can be reduced to 3 or 4 dimensions (which are composed of linear combinations of many of the original wavelengths) while preserving virtually all of the spectral information. Clustering algorithms can then readily work on such a reduced dataset to identify meaningful spectral clusters, although some techniques, such as support vector machines<sup>47</sup> are designed to use the original full feature space. A large variety of clustering methods, including iterative, analytical, neural net, fuzzy logic and genetic algorithm-based approaches, both published and proprietary, have been developed, whose description and virtues are beyond the scope of this review. A number of these tools are available as part of the software resources identified at the beginning of this section.

*Combined spectral and spatial analysis:* All the tools described above are designed to work only on the spectral content of the datacube. Remarkably, the pixels could be randomly scrambled, and if their associated spectra were preserved, analysis of the resulting scrambled images by the purely spectral-based algorithms would be unaffected. Obviously, a more powerful approach would somehow combine the rich spatial information present in the images, with the spectral data. This is an evolving field with on-going attempts to adapt remote-sensing expertise to problems in biomedical imaging.

## Applications

There are a number of areas for which spectral imaging holds out promise. This section will concentrate on applications involving microscopy and visual light, while touching on applications in other areas. In microscopy, the goal can be variously the spectral measurements of natural chromophores or environmentally sensitive indicator molecules (**imaging spectroscopy**), the detection and discrimination of multiple analytes (**multiplex imaging**), and/or the analysis of complex scenes (**spectral segmentation and morphometry**); these functions can be combined. It can thus serve as a bridge between the morphological (the traditional strength of pathology) and the molecular.

**Imaging spectroscopy:** Conceptually, the most straightforward application of spectral imaging involves the simple acquisition of spectra from naturally occurring or adventitious chromophores within a sample. Potential uses, in biomedicine, include the characterization of different melanin moieties in normal skin, dysplastic and malignant pigmented lesions, discrimination between oxy- and deoxyhemoglobin, or in the study of any pigments of interest in biological or non-biological samples. Comparison between the acquired spectra and pre-existing spectral libraries can be used to aid in the identification of specific species. An example of oxygenation-based studies of ischemic regions in a pig heart perfusion model is shown in Figure 6, which demonstrates application of macroscopic optics and a spectral range encompassing the near-IR.

Another use of spectral imaging in which the acquired spectrum has intrinsic importance is the detection of spectral shifts in (typically fluorescent) indicator dyes. Ion-sensitive dyes that shift their emission maxima in response to changing ion concentrations are well known but are not as frequently

used as dyes that change their excitation profile, in part because it has been easier to switch rapidly between excitation wavelengths than to do the same on the emission side. Emission-responsive dyes, such as Indo-1, SNARF-1, Acridine Orange, and Nile Red, can be excited at a single wavelength and their emission behavior monitored using either high-resolution or spectroscopy or by detecting intensities at only two or perhaps more specific wavelength ranges. An example using propidium iodide, which is sensitive to the relative proportion of DNA and RNA in a specimen, is shown in Figure 7, which compares 3 samples of yeast under 3 different experimental conditions. Spectral shifts, highlighted using principal components analysis (PCA), identify yeast in each class. Such small spectral shifts are easily separated by data from an image cube, but are not separable by filters without significant cross talk.

For ratio-based ion-sensitive imaging approaches, one would ideally wish to monitor emission at a number of wavelengths simultaneously, rather than sequentially, to obtain an instantaneous pixel-by-pixel measure of ion concentration. While LCTFs can be configured to switch between wavelengths with a switching time of 1-5 ms, and AOTFs in around 30 microseconds, these still represent serial measurements. Simultaneous measures can be achieved either by using the CTIS approach described above, or by using beam-splitters and interference filters to direct light with the desired wavelengths to one or more detectors in parallel. A commercial device that sends up to 4 images at different wavelengths simultaneously to a single detector is available from Optical Insights. To our knowledge, a comparison of the light efficiency and signal-to-noise capabilities of these different approaches has not yet been done.

**Multiplex imaging, including immunohistochemistry and in-situ hybridizations:** Spectral imaging on an analytic level facilitates multiprobe detection techniques for proteins, RNA and DNA. Histochemical, immunohistochemical, immunofluorescent and fluorescent molecular probes bind specifically to intra- or extracellular components and can be visualized with either fluorescence or bright-field (transmission) optics. Ideally, one would like to apply more than one specific probe at a time.

**Spectral Karyotyping:** Pioneering work in spectral karyotyping (SKY) using combinatorial labeling of metaphase chromosomes<sup>48</sup> allowed non-ambiguous identification of 27 chromosomes or chromosome pairs. This approach has been commercialized by Applied Spectral Imaging (Figure 8). Similar approaches using multiple fixed filter sets (M-FISH) have been described by David Ward and colleagues<sup>8</sup>.

**Immunofluorescence:** Multi-probe immunophenotyping has become widely used in evaluation of hematological malignancies, with four or even as high as 8 fluorescent signals being discriminated with sophisticated flow cytometry instruments<sup>49</sup>. The imaging approach to molecular characterization improves on flow cytometry in its ability to visualize the cells under study directly, to localize (and co-localize) cellular features, to count discrete objects on a per-cell basis and, in tissue sections, to allow correlation with tissue microarchitecture. Using more than 3 or at most 4 labels simultaneously in the absence of spectral imaging tools is currently difficult because of the problem of spectral overlap: it is not easy to prevent signal from one dye “leaking” into the spectral channel of another, and the problem becomes intractable for conventional interference filter-sets as the number of dyes is increased

<sup>50</sup>. Using spectral imaging, seven labels have been successfully discriminated<sup>51</sup>. Similar approaches can be used with multiple cell-compartment dyes. One problem with immunofluorescence is the interference of autofluorescence, which can be particularly troubling when formalin-fixed tissues are being examined. Other troubling specimens include many plant samples, insects, and *C. elegans* nematodes. One solution to autofluorescence difficulties is to shift the excitation and emission wavelengths into the red and far-red, where autofluorescence is far less intense. If that is not possible, then spectral imaging can be used to separate the unwanted autofluorescence signal from that of specific fluorescent dyes (Figure 9). In this approach, autofluorescence is treated as another spectral feature, as if it were a fluorescent probe.

**Immunohistochemistry:** More popular in clinical applications than immunofluorescence, IHC is widely used clinically for the detection of diagnostically or prognostically significant molecules in or on cells. In the past two decades the technique has become central to the practice of oncologic pathology<sup>52</sup> since it can distinguish between look-alike lesions (mesothelioma vs. carcinoma, for example), or divine the cellular lineage of extremely undifferentiated neoplasms (lymphoma vs. other so-called “small blue cell” tumors). It can also be used to highlight the presence of otherwise easily overlooked microscopic foci of tumor, such as micrometastases lurking in lymph nodes, and can be used to measure quantitatively the levels of diagnostically or prognostically important markers such as estrogen- and progesterone-receptors, Her2-neu, p53, ki-67, and a host of others<sup>53</sup>. Under some clinical circumstances, and often in research situations, double- or triple-staining single slides with different chromophore-coupled antibodies may be desirable. Triple-staining procedures are not often performed because of technical difficulties; however, with the advent of programmable staining systems, complex staining protocols may become less of a hindrance. Despite the non-linear effects of enzyme amplification, immunohistochemistry can be made quantitative, if precautions are taken<sup>54, 55</sup>. The major problem is that it is hard to determine visually where and to what extent the different stains may physically overlap when there may be co-expression of 2 or more analytes in the same cellular compartment. Spectral imaging can overcome this difficulty, even in the presence of considerable spectral overlap with the chromogens. Figure 10 demonstrates spectral unmixing of a triple-stained breast cancer sample. This specimen was probed with an anti-progesterone receptor (PR) immunostain coupled to a brown chromogen (DAB) and an anti-estrogen receptor (ER) immunostain coupled to a red chromogen (Fast Red); all nuclei were counterstained with a fairly dark hematoxylin wash. The RGB image reveals how difficult it is to determine by eye which cells are expressing PR, which ER and which both. After converting the image to OD, and using previously determined spectra for linear unmixing, separate images demonstrating localization of the PR, ER and hematoxylin stains are shown.

**FISH and TRISH:** In situ hybridization (ISH) has proven to be an invaluable molecular tool in research and diagnosis and has enabled major strides to be taken in the fields of gene structure and expression at the level of individual cells and in complex tissues. To date, the vast majority of ISH applications have relied on fluorescence readout systems because of their sensitivity, spatial resolution, relative simplicity, and easy adaptation to multicolor and quantitative methods. As noted above, it can be difficult using conventional filter sets to image multiple fluors simultaneously. With spectral imaging, it is possible to visualize 6 or more probes simultaneously (Figure 11) although similar feats can be accomplished using multiple filter cube sets and cross-talk correction (Larry Morrison, personal communication). As noted above<sup>21,22,23</sup>, issues of speed and signal-to-noise with the various approaches

have aroused some degree of controversy. In any event, FISH-based techniques have proven to be somewhat problematic in the clinical arena. Drawbacks include the disadvantage that most fluorescent signals fade upon exposure to light and during storage, interference by autofluorescence (which can be severe in formaldehyde-fixed tissues), and the cost of the microscopic and imaging equipment needed (not to mention the inconvenience of having to dim the lights around the imaging station). In addition, it is difficult to combine FISH with routine histopathological stains that can reveal the morphological context of the images.

Some of these difficulties have recently been overcome with the development of non-fading, brightfield detection methods for ISH signals<sup>56, 57, 58</sup>. Signals can readily be detected in tissue sections, which can also be counterstained with hematoxylin or other general histology stains. Finally, brightfield, or transmission-ISH (TRISH) can be combined with immunohistochemistry to provide truly multiparameter molecular characterization. An example of spectrally unmixed 3-color TRISH is shown in Figure 12 which includes an example of spectrally resolving physically overlapped centromeric chromosome probes.

### **Spectral segmentation and morphometry:**

Prostate cancer cells can be spectrally detected in images of prostate biopsy tissue stained with hematoxylin and eosin. This capability could be useful, for example, in automated screening of prostate “chips” removed for benign prostatic hyperplasia. Large volumes of tissue have to be examined in a search for potentially tiny foci of clinically unsuspected cancer. Figure 13 demonstrates that it is possible to spectrally separate malignant and normal epithelial cells, and to detect basal cells as well (these are a second cell layer found in normal prostate glands but absent in cancer). The segmentation is not perfect. Some of the imperfections (such as isolated misclassified pixels) can be suppressed using image-processing techniques. However, the limitations in the present case include the fact that the relatively unsophisticated minimum square error classification algorithm was used. More generally, it is likely that the stains, hematoxylin and eosin—convenient, ubiquitous and used for generations—may not be the optimal choice for spectral analysis of tissue.

Another demonstration of spectral classification (Figure 14) is provided by Malik and his colleagues, who used spectral characteristics to distinguish between morphologically similar circulating B-cell lymphocytic leukemia cells and normal lymphocytes<sup>59</sup>. These authors also showed how spectral tools can be used to highlight morphological features that can then be used to further characterize cells or tissues (Figure 14).

**Conclusion:** Fueled by rapid advances in instrumentation, software and algorithmic developments, novel dyes and chromogens, improvements in sample processing, and, stimulated by the genomics revolution, a need to increase throughput and multiplexing capabilities, spectral imaging is poised to make an ever-increasing contribution to biomedicine and related arts.

This research was carried out partially at the Jet Propulsion Laboratory, California Institute of Technology, under a contract with the National Aeronautics and Space Administration

## References

- <sup>1</sup> Kruse, F. A., Analysis of AVIRIS data for the northern Death Valley region, California/Nevada, *Proceedings of the Second AVIRIS Workshop*, JPL publication 90-54, Pasadena, 1990.
- <sup>2</sup> Johnson, L. F., F. Baret and D. Peterson, Oregon transect: comparison of leaf-level with canopy-level and modeled reflectance, *Summaries of the Third Annual JPL Airborne Geoscience Workshop*, JPL publication 92-14, volume 1, 113, Pasadena, 1992.
- <sup>3</sup> Fitzgerald, G. J., Maas, S. J., and DeTar, W. R., Early detection of spider mites in cotton using multispectral remote sensing, *Beltwide Cotton Conference*, Orlando, 1999
- <sup>4</sup> B.M. Abdulrauf, B.M, Stranc, M. F., Sowa, M.G, Germscheid, S. L. and Mantsch, H. H., a novel approach in the evaluation of flap failure using near ir spectroscopy and imaging, *Plastic Reconstructive Surgery* **8**, 68-72, 2000.
- <sup>5</sup> Sowa, M.G., Payette, J.R., Hewko, M.D. and Mantsch, H.H.. Visible - Near Infrared Multispectral Imaging of the Rat Dorsal Skin Flap, *Journal of Biomedical Optics* **4**, 474-481, 1999
- <sup>6</sup> Ruifrok, A. C. Quantification of immunohistochemical staining by color translation and automated thresholding, *Anal Quant Cytol Histol* **19**, 107-113, 1997
- <sup>7</sup> Ruifrok, A. C. and Johnston, D.A., Quantification of histochemical staining by color deconvolution, *Anal Quant Cytol Histol* **4**, 291-299, 2001
- <sup>8</sup> Speicher, M.R., Ballard, S. G. and Ward, D.C., Karyotyping human chromosomes by combinatorial multi-fluor FISH, *Nat. Gene.*, **4**, 368-75, 1996
- <sup>9</sup> Gat, N., Imaging spectroscopy using tunable filters: a review, *Proc. SPIE*, **4056**, 50-64, 2000
- <sup>10</sup> Morris, H.R, Hoyt, C.C and Treado, P.J., Imaging spectrometers for fluorescence and Raman microscopy – acousto-optic and liquid-crystal tunable filters, *Applied Spectroscopy*, **48**, 857-866, 1994.
- <sup>11</sup> Morris, H.R, Hoyt, C.C and Treado, P. Liquid crystal tunable filter Raman chemical imaging, *Applied Spectroscopy*, **50**, 805-811, 1996
- <sup>12</sup> Landsford, R, Bearman, G.H. and Fraser, S., Resolution of multiple green fluorescent protein color variants and dyes using two-photon microscopy and imaging spectroscopy. *Journal of Biomedical Optics*, **6**, 311-318, 2001.
- <sup>13</sup> Bearman, G.H, Spiro, S.I., Archeological applications of advanced imaging techniques, *Biblical Archeologist*, **59**, 56-66, 1996
- <sup>14</sup> Wachman, E.S, Niu, W. and Farkas, D.L., Imaging acousto-optic tunable filter with 0.35 micrometer spatial resolution, *Appl. Opt.*, **35**, 5220-5226, 1996
- <sup>15</sup> Lou Denes, CMRI, personal communication, 2001
- <sup>16</sup> [www.lightforminc.com](http://www.lightforminc.com)
- <sup>17</sup> Garini, Y., Katzir, N, Cabib, D., Buckwald, B., Soenksen, D. and Z. Malik, Spectral Bio-Imaging, in *Fluorescence Imaging Spectroscopy and Microscopy, Chemical Analysis Series 137*, Wiley and Sons, 1996
- <sup>18</sup> Schröck, E., S. du Manoir, T. Veldman, T., Schoell, D., Wienberg, J., Ferguson-Smith, M. A., Ning, Y., Ledbetter, D. H., Bar-Am, I., Soenksen, D., Garini, Y. and Ried, T., Multicolor spectral karyotyping of human chromosomes, *Science*, **26**, 494-497, 1996
- <sup>19</sup> Malik, Z, Cabib, D., Buckwald, R., Talmi, R., Garini, Y., and Lipson, S., Fourier transform multipixel spectroscopy for quantitative cytology, *J. Microscopy*, **182**, 133-140, 1996
- <sup>20</sup> Itoh, K., Watanabe, W. and Masuda, Y., Parallelisms in interferometric fast spectral imaging, *Proc. SPIE* **3261**, 278-288, 1998
- <sup>21</sup> Garini, Y., Gil, A., Bar-Am, I., Cabib, D. and Katzir, N., Signal to noise analysis of multiple color fluorescence imaging microscopy, *Cytometry*, **35**, 214-26, 1999
- <sup>22</sup> Castleman, K.R., Eils, R., Morrison, L., Piper, J., Saracoglu, K., Schulze, M.A., Speicher, M.R. Classification accuracy in multiple color fluorescence imaging microscopy, *Cytometry* **41**, 139-147 2000
- <sup>23</sup> Miller, P. and Harvey, A., Signal-to-noise analysis of various imaging systems, *Proc. SPIE*, **4259**, 16-21, 2001
- <sup>24</sup> Herman P., Malak H., Moore W. E. and Vecer J., Compact hyperspectral imager (HSI) for low light applications, *Proc. SPIE*, **4259**, 8-16, 2001
- <sup>25</sup> Okamoto, T. and Yamaguchi, I., Simultaneous acquisition of spectral image information, *Opt. Lett.* **16**, 1277-1279, 1991
- <sup>26</sup> Descour, M., Non-scanning Imaging Spectrometry, Ph.D. Dissertation, University of Arizona, 1994.
- <sup>27</sup> Volin, C.E., Ford, B.K., Descour, M.R., Wilson, D.W., Maker, P.M., Bearman, G.H., High speed spectral imager for imaging transient fluorescence phenomena, *Applied Optics* **37**, 8112-8119, 1998
- <sup>28</sup> D. Wilson, D, Maker, P. and Muller, R., Binary optic reflection grating for an imaging spectrometer, *Diffraction and Holographic Optics Technology III*, SPIE **2689**, 255-267, 1996
- <sup>29</sup> Ford, B.K, Volin, C.E, Murphy, S.M, Lynch, R.M. and Descour, M.R, Computed tomography-based spectral imaging for fluorescence microscopy, *Biophys J.*, **80**, 986-93, 2001

- <sup>30</sup> de la Iglesia, F., Haskins, J., Farkas, D. and Bearman, G., Coherent multi-probes and quantitative spectroscopic multimode microscopy for the study of simultaneous intracellular events, *International Society of Analytical Cytology, 20<sup>th</sup> Congress*, Montpellier, June, 2000
- <sup>31</sup> Treado, P.J. and Morris, M.D, Multichannel Hadamard transform Raman microscopy, *Appl. Spectrosc.* **44**, 1-4, 1990
- <sup>32</sup> Hanley, Q.S, Verveer, P.J. and Jovin, T.M, Spectral imaging in a programmable array microscope by Hadamard transform fluorescence spectroscopy, *Appl. Spectrosc.* **53**, 1-10, 1999
- <sup>33</sup> Miller, P.J. and Levenson, R., Beyond image cubes: an agile lamp for practical 100% photon-efficient spectral imaging, *Proc. SPIE*, **4259**, 1-7, 2001
- <sup>34</sup> <http://www.ece.purdue.edu/~biehl/MultiSpec/>
- <sup>35</sup> Perkins, S.J., Theiler, J., Brumby, S.P., Harvey, N.R., Porter, R.B., Szymanski, J.J., Bloch, J.J. GENIE: A hybrid genetic algorithm for feature classification in multispectral images, *Proc. SPIE* **4120**, 52-62, 2000
- <sup>36</sup> de Wolf, G. and van Vliet, L. J., Design of a four channel spectral analyzer to resolve linear combinations of two fluorescent spectra, *Proc. SPIE* **3920**, 21-29, 2000
- <sup>37</sup> Jimenez, L. O. and Landgrebe, D. A. Supervised classification in high dimensional space: Geometric, statistical, and asymptotical properties of multivariate data, *IEEE Transactions on Systems, Man, and Cybernetics, Part C: Applications and Reviews* **28**, 39-54, 1998
- <sup>38</sup> Ornberg, R. L., Woerner, B. M. and Edwards, D. A., Analysis of stained objects in histological sections by spectral imaging and differential absorption, *J Histochem Cytochem* **47**, 1307-1314, 1999
- <sup>39</sup> Mark, H. L. and Tunnell, D. Qualitative near-infrared reflectance analysis using Mahalanobis distances. *Anal. Chem.* **57**, 1449-1456, 1985
- <sup>40</sup> Kruse, F. A., Lefdooff, A. B., Boardman, J. W., Heidebrecht, K. B., Shapiro, A. T., Barloon, J. P. and Goetz, A. F., The spectral image processing system (SIPS)-- Interactive visualization and analysis of imaging spectrometer data, *Remote Sensing Environ.* **44**, 145-163, 1993
- <sup>41</sup> Harsanyi, J. C. and Chang, C. I. Hyperspectral image classification and dimensionality reduction: An orthogonal subspace projection approach. *IEEE Trans. Geosci. Remote Sens.* **32**, 779-785, 1994
- <sup>42</sup> Garini, Y., Katzir, N., Cabib, D., Buckwald, R. A., Soenksen, D. G. and Malik, Z., Spectral Bio-Imaging, in *Fluorescence Imaging Spectroscopy and Microscopy*. X. F. Wang and B. Herman, eds. John Wiley & Sons, Inc., 1996
- <sup>43</sup> Farkas, D. L., Du, C., Fisher, G. W., Lau, C., Niu, W., Wachman, E. S. and Levenson, R. M. Non-invasive image acquisition and advanced processing in optical bioimaging, *Comput Med Imaging Graph* **22**, 89-102, 1998
- <sup>44</sup> Winter, M. E., Fast autonomous spectral end-member determination in hyperspectral data, Proceedings of the Thirteenth International Conference on Applied Geologic Remote Sensing, Vancouver, B.C, Canada 2: 337-344, 1999
- <sup>45</sup> Landgrebe, D. A. Information extraction principles and methods for multispectral and hyperspectral image data, in *Information Processing for Remote Sensing*. C. H. Chen, ed., World Scientific, River Edge, NJ, 2000.
- <sup>46</sup> Mansfield, J. R., Sowa, M.G., Payette, J.R., Abdulrauf, B., Stranc, M.F., Mantsch, H.H., Tissue viability by multispectral near infrared imaging: a fuzzy C-means clustering analysis, *IEEE Trans Med Imaging* **17**, 1011-1018, 1998
- <sup>47</sup> S. Perkins, N.R. Harvey, S.P. Brumby and K. Lacker. Support vector machines for broad area feature extraction in remotely sensed images, *Proc. SPIE* **4381**, 268-295, 2001
- <sup>48</sup> Ried, T., Liyanage, M., du Manoir, S., Heselmeyer, K., Auer, G., Macville, M., and Schrock, E., Tumor cytogenetics revisited: comparative genomic hybridization and spectral karyotyping, *J Mol Med* **75**, 801-814, 1997
- <sup>49</sup> Roederer, M., De Rosa, S., Gerstein, R., Anderson, M., Bigos, M., Stovel, R., Nozaki, T., Parks, D. and Herzenberg, L. 8 color, 10-parameter flow cytometry to elucidate complex leukocyte heterogeneity. *Cytometry* **29**, 328-339, 1997
- <sup>50</sup> Brelje, T.C., Wessendorf, M.W. and Sorenson, R.L. Multicolor laser scanning confocal immunofluorescence microscopy: practical application and limitations, In *Cell Biological Applications of Confocal Microscopy*, Matsumoto, B., ed., Vol. 38, pp. 97-181, Academic Press, San Diego, 1993
- <sup>51</sup> Tsurui, H., Nishimura, H., Hattori, S., Hirose, S., Okumura, K. and Shirai, T., Seven-color fluorescence imaging of tissue samples based on Fourier spectroscopy and singular value decomposition, *J Histochem Cytochem* **48**, 653-662, 2000
- <sup>52</sup> Taylor, C. R. and Cote, R. J., Immunohistochemical markers of prognostic value in surgical pathology, *Histol Histopathol* **12**, 1039-10552, 1997
- <sup>53</sup> Albonico, G., Querzoli, P., Ferretti, S., Magri, E. and Nenci, I., Biophenotypes of breast carcinoma in situ defined by image analysis of biological parameters, *Pathol Res Pract* **192**, 117-123, 1996
- <sup>54</sup> Zhou, R., Parker, D. L. and Hammond, E. H., Quantitative peroxidase-antiperoxidase complex-substrate mass determination in tissue sections by a dual wavelength method, *Anal Quant Cytol Histol* **14**, 73-80, 1992
- <sup>55</sup> Fritz, P., Wu, X., Tuczec, H., Multhaupt, H. and Schwarzmann, P., Quantitation in immunohistochemistry. A research method or a diagnostic tool in surgical pathology? *Pathologica* **87**, 300-309, 1995
- <sup>56</sup> Speel, E. J., Ramaekers, F. C. and Hopman, A. H., Cytochemical detection systems for in situ hybridization, and the combination with immunocytochemistry: "Who is still afraid of red, green and blue?", *Histochem J* **27**, 833-858, 1996
- <sup>57</sup> Hopman, A. H., Claessen, S. and Speel, E. J., Multi-colour brightfield in situ hybridisation on tissue section, *Histochem Cell Biol* **108**, 291-298, 1998

<sup>58</sup> Speel, E. J., Hopman, A. H. and Komminoth, P., Amplification methods to increase the sensitivity of in situ hybridization: play card(s), *J Histochem Cytochem* **47**, 281-288, 1999

<sup>59</sup> Malik, Z., Rothmann, C., Cycowitz, T., Cycowitz, Z. J. and Cohen, A. M., Spectral morphometric characterization of B-CLL cells versus normal small lymphocytes, *J Histochem Cytochem* **46**: 1113-1118, 1998

## Figure captions for Biological Imaging Spectroscopy

Gregory Bearman, Jet Propulsion Laboratory, California Institute of Technology  
Richard Levenson, Cambridge Research and Instrumentation, Woburn, MA

Figure 1. An illustration of the basics of imaging spectroscopy. Multiple images of the same scene are acquired at many different wavelengths, as schematically shown. The spectrum of any pixel in the image can be obtained by plotting signal against wavelength over the spectral range available. The images here are from a human brain, imaged after being frozen. The white areas on the side are the frozen matrix that maintains the brain's shape and provide some hydration.

Figure 2. A schematic illustration of the various approaches to acquiring spectral image cubes. In each case, it is shown how a technique slices through an  $(x,y,\lambda)$  data set.

Figure 3. Operation of a liquid crystal tunable filter. Each successive stage of the filter is used to help cancel unwanted transmission of the previous stages. For a multistage filter, the final transmission is at a fixed peak. Tunability is introduced via the liquid crystal layer of 3b, which voltage tunes the retardance of each stage. This tunability is used to move the band of constructive interference to the desired wavelength.

Figure 4. Operation of an acousto-optic tunable filter. An acoustic wave, launched into a crystal by a transducer, produces a Bragg grating that diffracts the incident light. There are three output beams, a undiffracted beam and two monochromatic ones, one polarized vertical and the other horizontal.

Figure 5. Operation of the Microcosm imaging spectrometer.

Figure 6. Computed Tomographic Imaging Spectrometer. A diffractive grating, written by e-beam lithography, multiplexes the spatial and spectral information of a single pixel onto many sensor pixels. The observed scene is in 5a, consisting of 3 color LEDs, a HeNe laser spot and an 8-segment indicator. In 5b is shown the resulting image from the focal plane. There is a zero order image, 5c, that can be used for focusing as well as providing an initial starting point for the reconstruction of the image cube. Recovered spectra are shown in 5d.

Figure 7. Near-Infrared spectroscopy can detect variations in tissue oxygen levels by means of hemoglobin absorption peaks (lower right). Wavelength control was achieved using a liquid crystal tunable filter in front of a CCD. Pseudocolor highlights left ventricle deoxygenation during occlusion of the artery that normally supplies it. Unpublished images courtesy of Henry Mantsch, National Research Council, Winnipeg, Canada.

Figure 8. Spectral imaging and image segmentation of yeast cells stained with propidium iodide (PI). Top left: Composite containing 3 panels of PI-stained yeast cells imaged under 3 conditions: immediately after transfer of yeast to new medium, after 5 hours of culture, and after 5 hours of culture plus the addition of RNase. Bottom left: Spectra

from yeast in each culture condition obtained by imaging using a liquid crystal tunable filter. Small differences in peak position and shoulder configuration are visible. Bottom right: Scatter-plot of the spectral image after principal components analysis. 3 clusters are circled and the pixels contained in each cluster pseudocolored. Top right: result of mapping pseudocolored PCA clusters back to the original image, resulting in robust segmentation. RL, CRI, Inc.

Figure 9. Comprehensive cytogenetic analysis of a metaphase spread from a child (CK1) with dysmorphic features and developmental delay resembling an 18q-syndrome. Spectral karyotyping (SKY) was performed on a metaphase spread. The multicolor hybridization clearly reveals an aberrant chromosome (*arrow*) that contains chromosomes 18 (*red*) and X (*dark green*) material. The G-banding interpretation of a normal male karyotype (46,XY) was therefore corrected after SKY to 46,XY, der(18)t(X;18)(?;q23). (Reprinted with permission from Schrock, E., Veldman, T., Padilla-Nash, H. et al., Spectral karyotyping refines cytogenetic diagnostics of constitutional chromosomal abnormalities, *Hum Genet* **101**: 255-262, 1997)

Figure 10. Removal of autofluorescence using pixel unmixing. Top panel: Composite of 6 neurons in formalin-fixed, paraffin-embedded human brain stained with anti-GDNF labeled with Cy2. The bulk of the fluorescent signal is autofluorescence. Center panel: the single positively stained neuron is separated from the abundant autofluorescence using pixel unmixing (unmixing spectra shown in the insert). Bottom panel: Cy2 signal (in green) overlain on top of the autofluorescence signal (in gray). Sample courtesy Neelima Chauhan and George Siegel; analysis: RL, CRI, Inc.

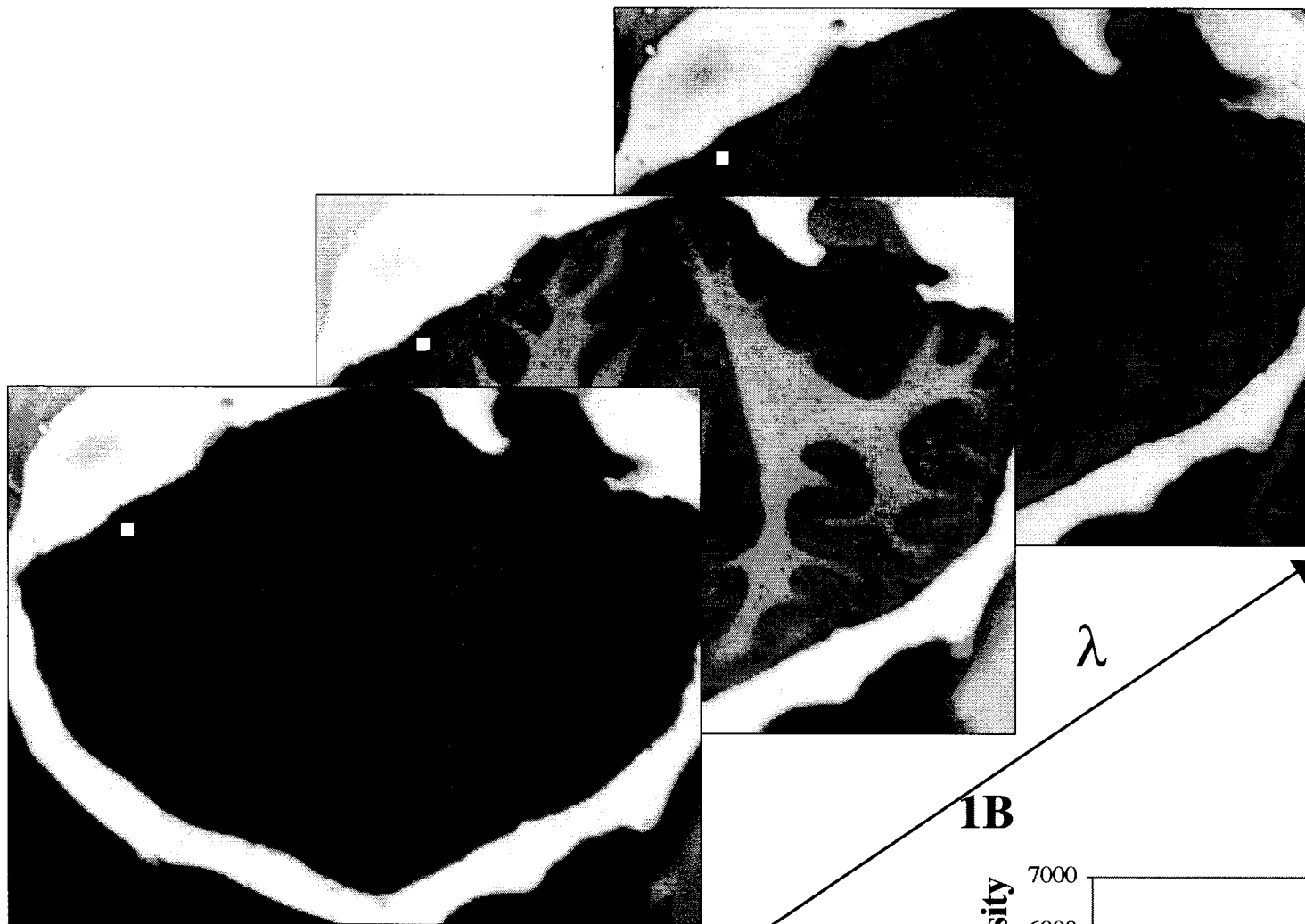
Figure 11. Multicolor immunohistochemistry and spectral unmixing. Top left: RGB image of a cluster of breast cancer cells stained for the presence of estrogen receptor (ER, red), progesterone receptor (PR, brown); nuclei are counterstained with hematoxylin (blue). It is difficult to determine how much of each antigen is present in the cancer cell nuclei. After collecting a spectral stack, the signals corresponding to nucleus, ER and PR are spectrally unmixed and shown in separate images. Bottom right shows where ER and PR are co-expressed (yellow signal). Sample courtesy Dako, Inc; analysis: RL, CRI, Inc.

Figure 12. Spectral unmixing of transmission in-situ hybridization (TRISH). Nuclei of cytospun bladder carcinoma cells probed for 3 chromosome centromeres. Detection was performed using DAB, New Fuchsin and TMB as chromogens. Lower panel: Spectral unmixing reveals overlap of brown and red signals (pseudocolored as green and red, respectively). The arrow points to a yellow spot representing the overlap. Sample courtesy Anton Hopman, Univ. Maastricht; analysis: RL, CRI, Inc.

Figure 13. Spectral segmentation of hematoxylin- and eosin-stained prostate cancer specimen. Left: RGB image of prostate cancer (Ca) and normal (NI) glands. The normal glands are lined with a double cell layer consisting of epithelial and basal cells; the cancerous glands have a single cell layer. Right: result of spectral segmentation using spectra chosen manually from representative pixels in the image and a minimum square error classification algorithm. The 2 cell layers (pseudocolored green and blue) are

spectrally distinct from one another and from the cancer cells (pseudocolored red).  
Analysis: RL, CRI, Inc.

Figure 14. Spectral classification and morphological analysis. Normal lymphocytes are compared to small B-cell lymphocytic leukemia cells, both stained with Giemsa. By eye these are virtually indistinguishable. Spectral classification, using the spectra shown in the lower right panel, reveals spectral differences in content and spatial distribution of the spectral features (top right and left panels). Lower left: spectral similarity mapping algorithms indicate more clearly the differences in distribution of spectral features in normal vs. lymphocytic leukemia cells. (Reprinted with permission from Malik, Z., Rothmann, C., Cycowitz, T., Cycowitz, Z. J. and Cohen, A. M., Spectral morphometric characterization of B-CLL cells versus normal small lymphocytes, *J Histochem Cytochem* **46**: 1113-1118, 1998)



**1B**

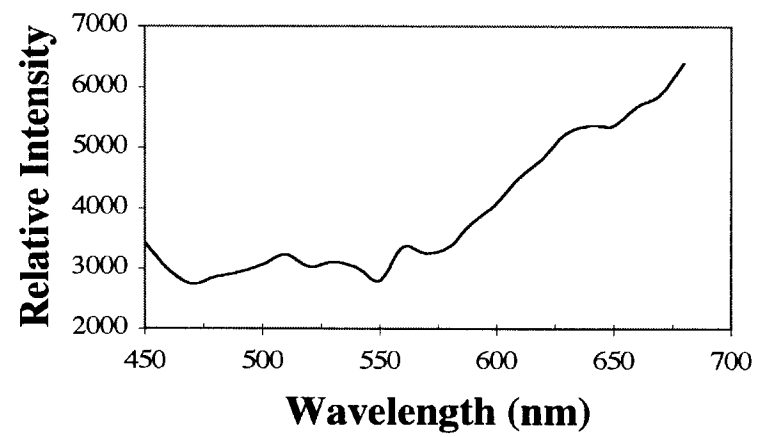
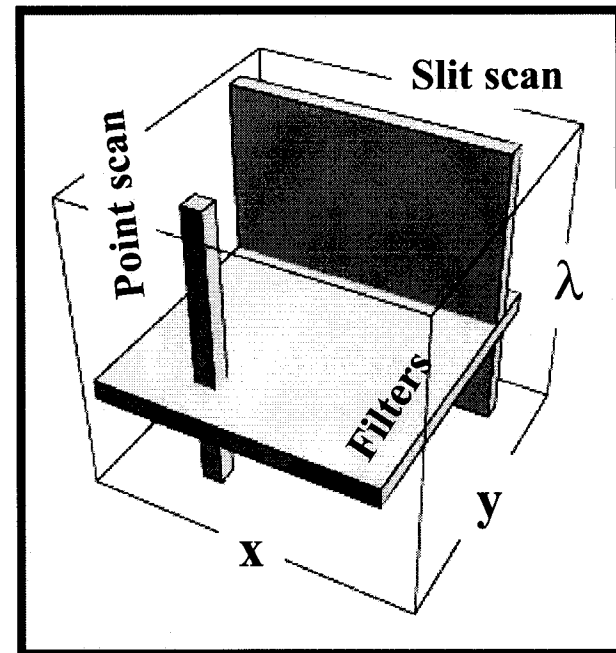


FIG. 1

# Spectral Imaging

- Cytogenetics and pathology
- Application to *in vivo* studies limited by temporal resolution
- Current methods - **scanning**
- **CTIS**: Simultaneously acquires spectral information from every position element within a 2-D FOV with high spatial and spectral resolution.



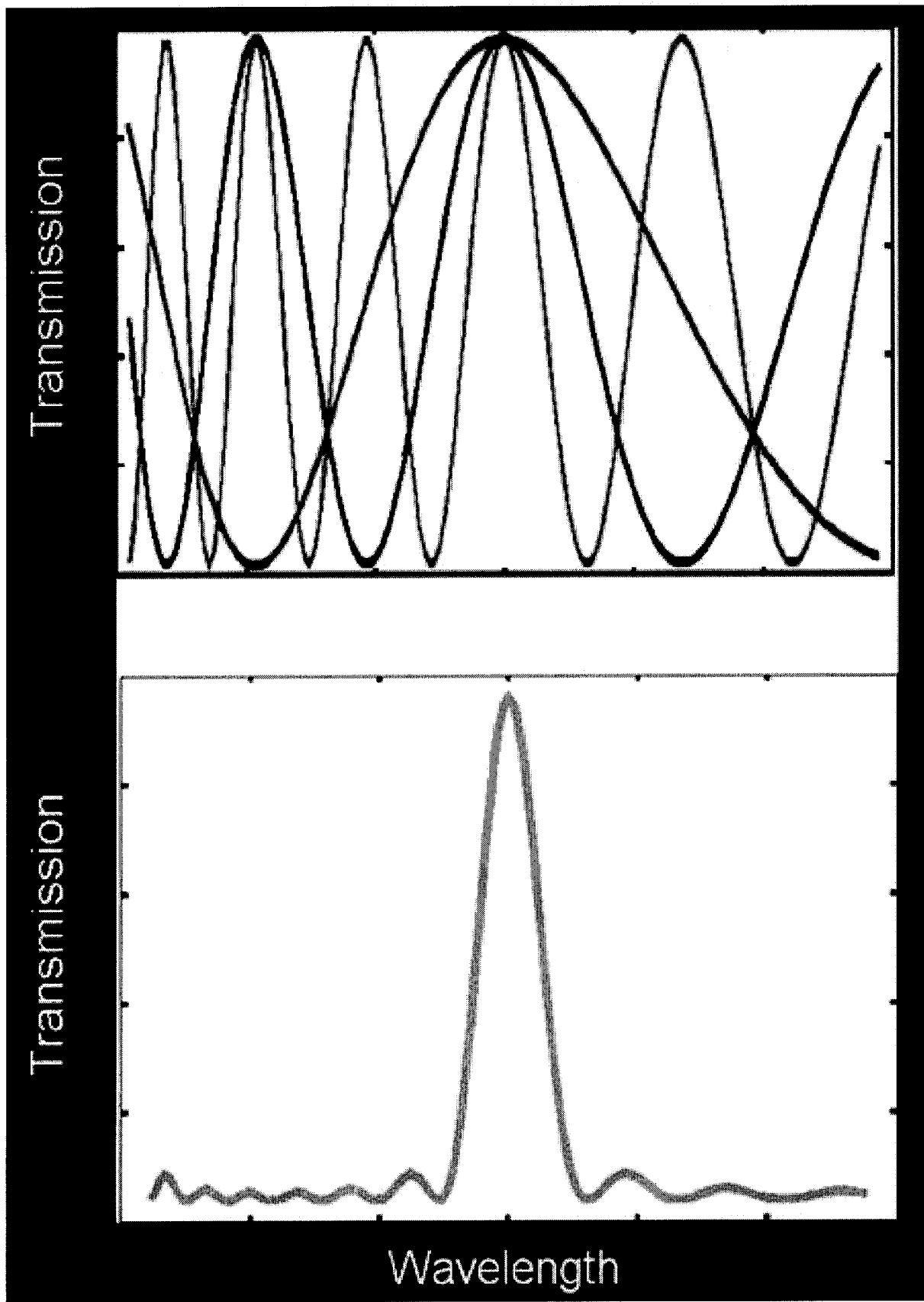
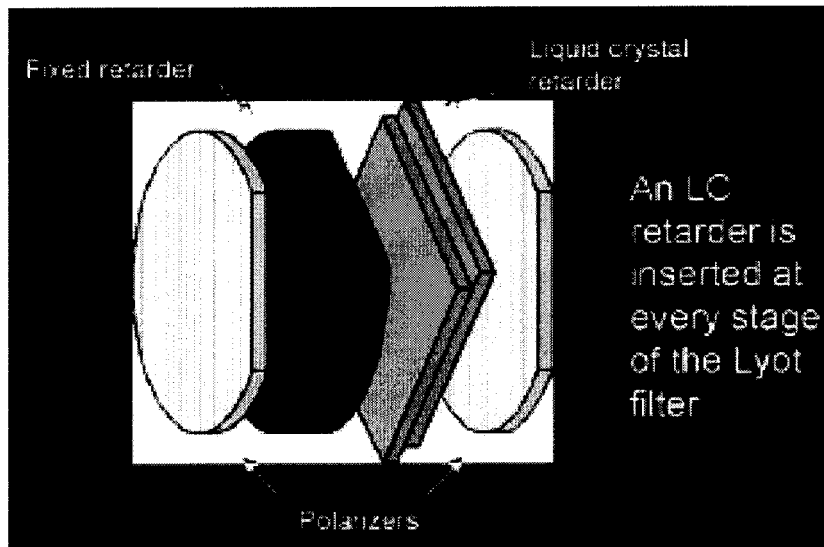
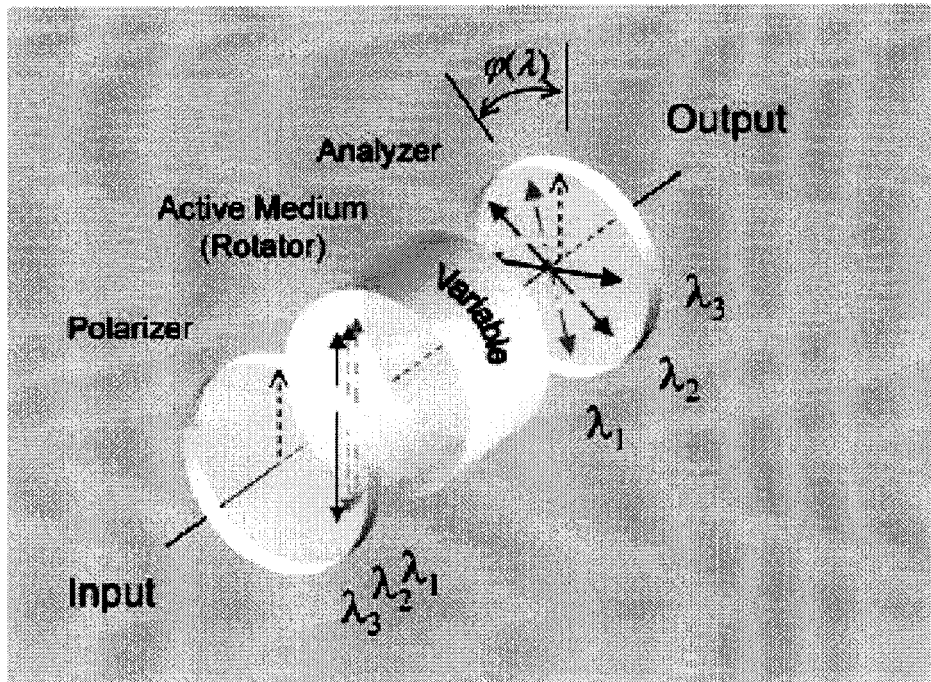


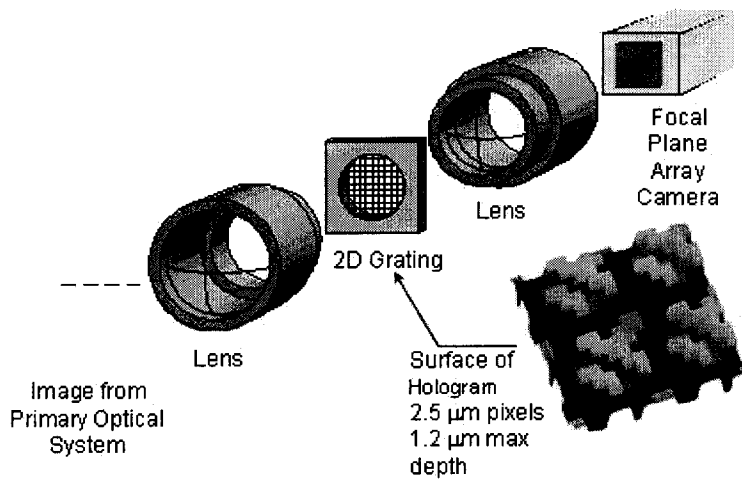
FIG. 3 LCTF transmission



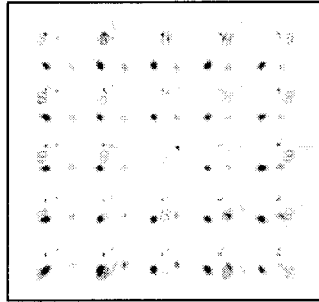
CRC\_figure\_3a\_LCTF stage.jpg



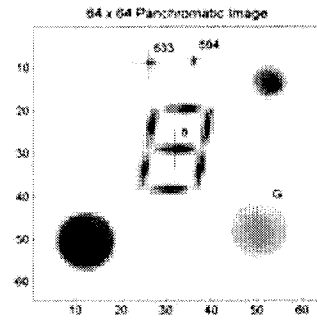
CRC\_Figure\_4\_Microcosm rotogram



Experimental Scene



Intensity on Focal Plane Array  
(Image taken in dark ambient)



Reconstructed Spatial-Spectral Scene

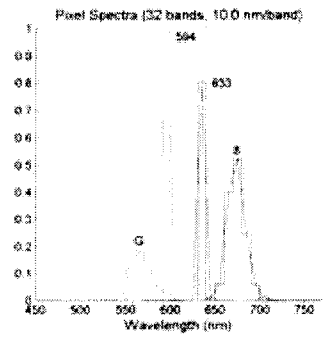


FIG. 5 CTIS.jpg

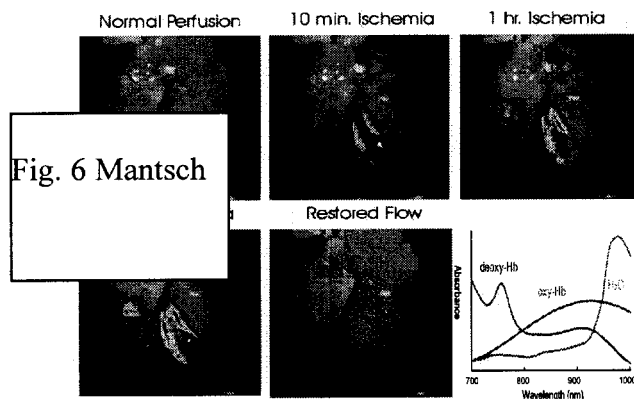


Fig. 6 Mantsch

**Near-Infrared spectroscopy can detect variations in tissue oxygen levels by means of hemoglobin absorption peaks**

Fig. 7  
Levenson

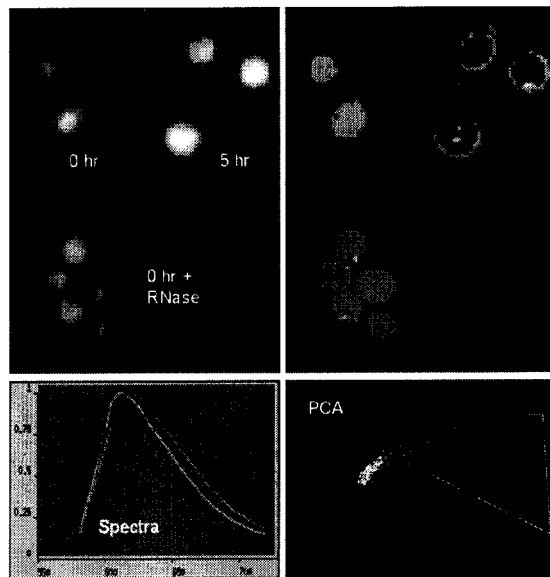


Fig. 8 Ried

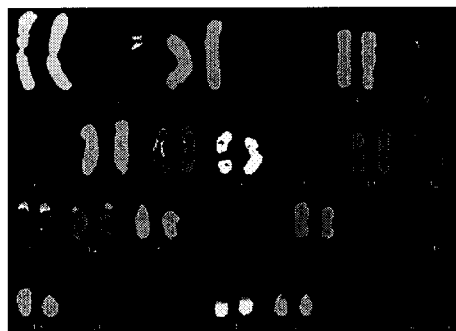
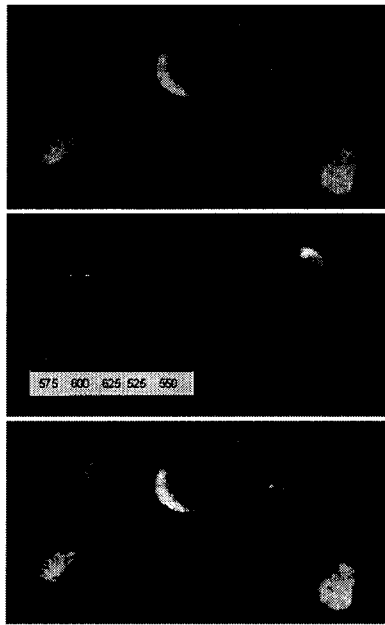


Fig 9.  
Levenson



Spectral analysis:  
Immunohistochemistry

Breast Tissue:  
Double stained  
Progesterone receptor: DAB  
Estrogen receptor: Fast Red  
Counterstain: hematoxylin

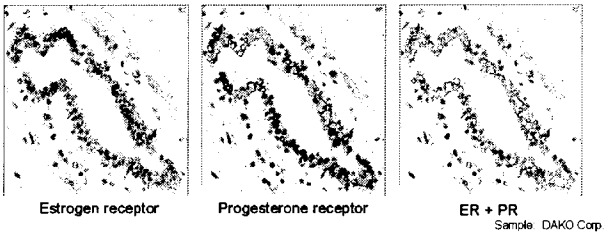
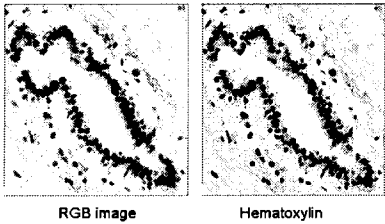
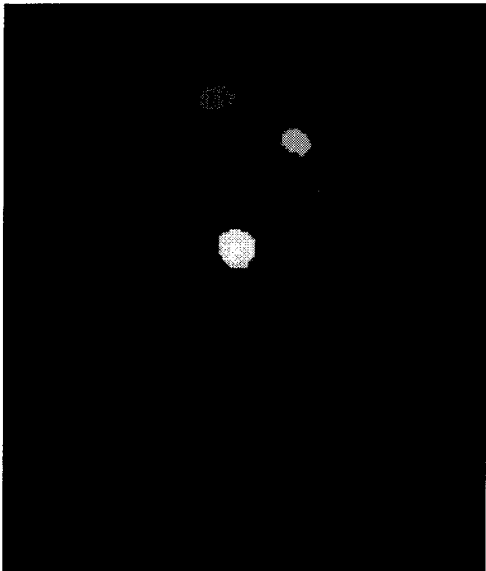


Fig. 10.  
Levenson

Fig. 11  
ASI



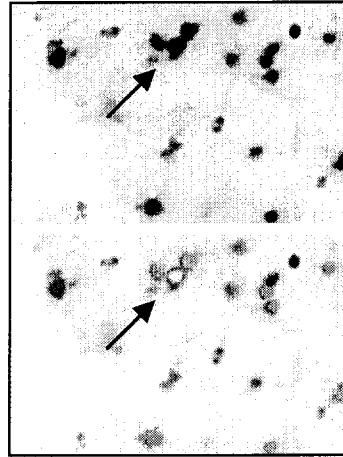


Fig. 12.  
Levenson

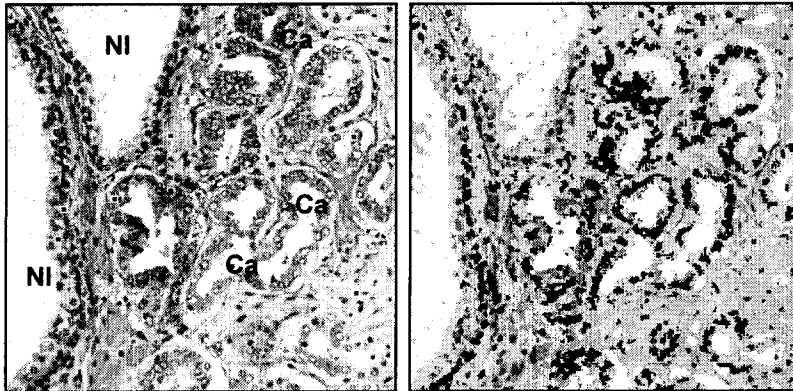


Fig. 13.  
Levenson

Fig 14. Malik

